Modelling the morphology of hydrides in fuel rod cladding under the conditions of the long-term bundle test in the framework of the SPIZWURZ project

MIKHAIL KOLESNIK, JURI STUCKERT, MIRCO GROSSE
Institute for Applied Materials, Karlsruhe Institute of Technology,
Kaiserstrasse 12, 76131 Karlsruhe – Germany

ABSTRACT

A long-term bundle tests lasting 250 days were conducted at the LICAS facility in the Karlsruhe Institute of Technology as part of the SPIZWURZ project. The pressurized fuel rod simulators with commercial prehydrided non-irradiated claddings were tested under conditions close to the ones of dry storage of spent nuclear fuel. This paper compares the morphology of hydrides observed after this testing with the results of numerical simulations. The morphology of the hydrides largely determines the fracture mode of hydrated zirconium alloys, as an interconnected network of hydrides can conduct a brittle crack leading to a critical embrittlement. The morphology of hydrides under experimental conditions has been simulated numerically using two approaches. The first approach involves solving a system of differential equations that considers the processes of dissolution, nucleation, and growth of hydrides. This method predicts the average values of the main hydride morphology parameters during heating and cooling, including orientation, average size, and spacing between hydrides. The second approach is the MORPHYD tool, which simulates the nucleation and growth of separated hydrides in a 3D domain. It allows predicting any morphology parameters, including hydride continuity metrics, which are widely used in practice. The MORPHYD tool simulates not only average values of the morphology parameters, but also their statistical distribution based on Monte Carlo method. It makes possible to estimate the probability of a local critical hydride embrittlement. Theoretical approaches showed acceptable agreement with experiments for several hydride morphology metrics. Further model adjustments are planned following the receipt of additional experimental data from SPIZWURZ project.

1. Introduction

One of the most deleterious physical processes limiting the safety regimes of spent nuclear fuel dry storage is hydride embrittlement of zirconium fuel rod cladding. Hydrogen in the cladding accumulated during normal operation of the nuclear fuel. Free hydrogen is a secondary product of water corrosion, which can be partially absorbed by the metal matrix. As a first approximation, the hydrogen concentration in zirconium alloys is approximately proportional to the oxide thickness [1]. Its level at the end of operation is determined by the burnup (operating time), the corrosion resistance of the alloy and the operating conditions (water chemistry, temperature and other factors determined by the reactor type). The hydrogen concentration in the metal matrix has a profile along the cladding length and for high burnup fuel the typical values are 150 – 650 ppm in Zirlo™ (68 – 70 GWd/MTU [2], [3], [4]), 200 – 550 ppm in Zircaloy-4 (50 – 67 GWd/MTU [2], [3]), 50 – 100 ppm in M5 (63 – 70 GWd/MTU [4]).

Brittle fracture of hydrogenated zirconium alloys in conditions typical for the lifetime of nuclear fuel is localized inside the hydride phase. There are three hydride embrittlement physical mechanisms in zirconium alloys [5]. (1) Hydrides can act as a nucleation site for fracture, specifically at points where the slip band of the metal matrix intersects a hydride surface. (2) Hydrides can provide pathways for brittle crack propagation with low fracture energy. (3) Hydrides can increase the non-homogeneity of ductile flow, thus leading to large internal strain localization. The second mechanism is closely related to the degree of hydride embrittlement and the morphology of hydrides. The formation of an interlinked hydride network is a necessary condition for the fully brittle fracture of hydrogenated zirconium alloy. This experimental fact provides grounds for approaches to predict the degree of hydride embrittlement based on the modelling of hydride morphology.

Hydrides exhibit a complex three-dimensional morphology, forming plate-like precipitates, as evidenced by published synchrotron X-ray tomography data [6]. In practice, the morphology of hydrides is typically investigated in a 2D approximation by cross-section micrography, and the morphology of hydrides can be described by a set of parameters, including the length of hydrides, their orientation, and the distance between hydrides. These parameters are determined by the metallurgical state of the alloy and the conditions of hydride nucleation and growth. The orientation of hydrides at zero or low external mechanical stresses is mainly determined by the texture of the alloy and is correlated with Kearns factors [7], [8]. When the stress exceeds the threshold, it becomes the main factor influencing orientation and hydride plates tend to orient perpendicular to the tensile stress [9]. The main factors determining the length of hydrides and the distance between them are the concentration of hydrogen in the hydride phase and the precipitation rate (which is often determined by the cooling rate and the microstructure) [10]. Under otherwise identical conditions, the metallurgical state also influences the size of hydrides. For example, equiaxed grains in the recrystallized samples lead to the precipitation of shorter hydrides compared to a stress-relieved structure [11].

The single morphology metrics discussed above only correlate with mechanical properties under specific conditions. The correlation of the RHF (Radial Hydride Fraction) is valid only for a certain hydrogen content. The hydrogen concentration in radial hydrides ignores the length of hydrides (strong parameter influencing brittleness). The maximal length of radial hydrides ignores the clustering effect when a few shorter hydrides can create a higher local embrittlement than the longer one. The length of radial hydrides per unit area ignores their size and distance between them. As a result, more universal metrics, characterizing the connectivity of the hydride network, have been developed. A number of connectivity metrics have been developed, which are a combination of basic morphology parameters. These metrics show stronger correlation with mechanical properties and lower dependence on experimental conditions. These include the radial hydride continuity factor (RHCF) [2], the hydride continuity coefficient (HCC) [12], [13], the accumulated hydride length (AHL) [14], the radial hydride continuous path (RHCP) [15]. Moreover, future hydride morphology analysis may extend to 3D analysis [16], which could provide further insight into the exhaustive metrics.

When applying morphology metrics in practice, it is important to consider that these metrics are local parameters that can vary throughout the sample volume. As an example, the statistical distribution of RHF and RHCP was numerically measured in [17]. As samples fracture at their weakest point, the embrittlement degree should be characterized by the highest local embrittlement degree and, thus, the highest value of the local morphology metric. Consequently, experimental studies of morphology and mechanical properties can face the problem of small samples. In order to ensure that the studied sample volume includes the worst local hydride morphology with a reasonable probability (for example, 99.99%), it must be large enough.

The basic theoretical models for predicting the morphology of hydrides focus on the simulation of the RHF metric. The classical approach assumes that the orientation of hydrides is determined by the ratio of the nucleation frequencies of hydrides with two different orientations [18]. It has been widely applied in kinetic models simulating RHF in fuel rod cladding [19], [20], [21], [22]. The alternative approach based on engineering correlations considers the stress threshold for reorientation as an alloy parameter and is also applied in

kinetic models simulating RHF [23], [24], [25]. Simulation of hydride mean length and spacing requires additional coupled modelling of nucleation and diffusion growth. This has been done in the classical nucleation theory approximation [19], [26]. Some hydride continuity metrics can be estimated if average values of hydride orientation, length and spacing are known. Alternatively, it can be a result of direct simulation of hydride nucleation and growth in the 3D domain [27], [28]. The statistical distribution of hydride metrics is modelled based on the Monte Carlo method and a statistically significant number of independent simulations [27], [28]. However, under the simplified assumption that the nucleation and growth of hydrides is independent of their neighbours, the statistical distribution of the hydride cluster length (the basis of the HCC and AHL morphology metrics) can be estimated analytically, as was done in the appendix of [27].

This paper describes application of two theoretical approaches for modelling hydride morphology in conditions of the SPIZWURZ bundle test simulating the long-term dry storage of spent nuclear fuel [29], [30]. The approaches allowed to predict main morphology metrics (including connectivity metrics) and their statistical distributions.

The SPIZWURZ project uses non-irradiated samples. Under conditions of safety and regulatory restrictions, limited technical capabilities and resources (time, human, financial and others), it allows an in-depth experimental study of the physical processes related to hydrogen behavior in zirconium alloys. The physical processes in irradiated samples, which are more relevant to the spent fuel storage problem, are generally the same. However, some differences in microstructure may influence hydride embrittlement degree, if all other conditions are equal. Firstly, neutron irradiation increases the solubility of hydrogen in zirconium alloys. The decrease in solubility temperature can be up to 30 – 100 ºC (for both dissolution and precipitation) depending on fluence, flux and irradiation temperature [31], [32], [33]. The mechanism is related to radiation-induced defects such as point defects [31], dislocation loops [34] and second phase particles with high density (for example, nanoscale Nb-enriched precipitates) [35], which act as traps for dissolved hydrogen atoms, inhibiting their mobility and participation in hydride precipitation/dissolution processes. High temperature annealing can recover solubility [32]. Under conditions typical of dry storage, the solubility for dissolution is expected to recover almost completely, while the solubility for precipitation is expected to recover only partially [33]. Secondly, irradiation can influence the morphology of hydrides. In [36] it was shown that the previous neutron irradiation of Zircaloy-4 samples makes the hydride morphology more disordered and after a thermomechanical cycle with external stresses of 150 MPa, both the RHF and the total hydride length per unit area are lower in irradiated samples than in unirradiated ones. On the contrary, according to [3] and [37] the irradiation effect in Zircaloy-4 is weak, and the difference of reorientation stress thresholds is within the experimental uncertainty. In M5 alloy, irradiation resulted in a reduction of the hydride reorientation threshold from ~ 75 MPa to ~ 50 MPa [38]. The effect of irradiation on hydride orientation and length is also assumed to be related to radiation-induced microstructural defects. For model development, this means that the parameters of the model related to microstructure and defining hydrogen solubility, hydride nucleation rate and sensitivity to stress reorientation may be different, but the main physically based equations are the same for irradiated and unirradiated samples. A detailed experimental study of non-irradiated samples allows the model to be verified in all relevant regimes and conditions. The physically based model can then be used to simulate irradiated samples if the model parameters have been calibrated with a limited number of experiments on irradiated samples.

2. Two models used for simulations

2.1 The model based on ODE system solution

The first model is a priori based on the numerical solution of the system of ordinary differential equations. The approach is able to simulate the evolution of the mean values of basic hydride morphology parameters, such as orientation, mean length of hydrides and mean inter-hydride distance during thermomechanical treatment. The model applied in the current simulations is based on the previously published one in [26], and here is only a brief description.

The current model incorporates the following physical processes: reorientation of hydrides under external conditions (stress and temperature), diffusional growth/dissolution of hydrides and precipitation of new hydrides. There are four independent variables: hydrogen concentration in solid solution C_s, the fraction of hydride precipitated as radially-oriented hydrides θ, and volume concentration of radial and tangential hydrides n_r, n_t.

The kinetic of hydrogen in solid solution is described as the relaxation of the hydrogen supersaturation with a characteristic time τ_0, as previously described in [21] and [26].

$$\frac{\mathrm{d}C_s}{\mathrm{d}t} - \frac{1}{\tau_0}\left(C_s - C_e\right) = 0 \tag{1}$$

where C_e – equilibrium solubility, which is different for growth (terminal solid solubility for precipitation, TSSP) and dissolution (terminal solid solubility for dissolution, TSSD); the corresponding correlations on temperature of TSSP(T) and TSSD(T) are assumed to be for Zircaloy-4 according to experimental data [39]. The characteristic time is determined as $\tau_0 = \Delta^2 / \alpha^2 D_{\mathrm{H}}$, where Δ – mean distance between hydrides, calculated with taking into account the amount of precipitated hydrogen, volume concentration and orientation of hydrides (more detailed in the Appendix A – C in [26]), $\alpha \sim 0.2$ – geometry factor, D_{H} – diffusion coefficient of hydrogen in zirconium alloy (diffusion coefficient according to experimental data [40] for Zircaloy-4 are used in the current simulations).

Nucleation process can be simulated in a classical heterogeneous approximation, where the nucleation rate R (the number of new hydrides nucleated in unit volume per second) is:

$$R = NZj^* \cdot \exp\left(-\Delta G^* / kT\right) \tag{2}$$

ΔG^* – Gibbs energy change due to nucleation of a hydride with the critical size, k – Boltzmann constant, T – temperature, N – density of nucleation sites, $j^* = 2\pi D_{\mathrm{H}} d^* \left(C_s - C_e\right)$ – the hydrogen flow to the spherical nucleus of the hydride with critical diameter d^* as the solution of a diffusional task in spherical symmetry, $Z = \left(\Delta G^* / 3\pi kTn^{*2}\right)^{1/2}$ – Zeldovich factor (according to Eq. 2.107 in [41]), where n^* – the number of atoms in the critical nucleus of hydride.

The Gibbs energy change encompasses a number of terms associated with mechanical, chemical and surface energy, as well as the energy of the defect at the nucleation site:

$$\Delta G^* = \Omega^* \left(g_m - \Delta\mu / v\right) + S^* \gamma - G_d \tag{3}$$

where Ω^*, S^* – volume and surface area of the critical nucleus; $g_m \approx \sigma_y \varepsilon$ – self mechanical deformation energy due to the volume dilatation with σ_y – yield stress, ε – volume dilatation; $\Delta\mu = \chi \cdot kT \cdot \ln\left(C_s / C_e\right)$ – chemical energy change per unit volume with χ – molar fraction of hydrogen in the hydride phase (χ = 1.6 for δ-$ZrH_{1.6}$); v – hydrogen atomic volume in hydride phase; γ – surface energy of the metal/hydride interphase; G_d – the defect energy of the current nucleation site. All of these parameters may be affected to varying degrees by the type of zirconium alloy, which may result in different metrics for different alloys.

Nucleation sites are inhomogeneities of the crystal lattice that are more preferable for the nucleation of new hydrides, as they have a lower energy barrier for nucleation. The nucleation sites can be triple points, grain boundaries, second phase particles' surface, intersections of dislocations and others. Different nucleation sites have different defect energy G_d in Eq. (3), corresponding to their defect type. In the current model, the defect energy G_d is assumed to have a normal distribution with a mean value and standard deviation defined by the user. Given the exponential dependence of the nucleation frequency on the Gibbs energy, it is assumed that nucleation sites with the highest defect energies are filled first. The lowest defect energy G_d^{occup} of occupied nucleation sites can be estimated by solving the following equation:

$$\frac{1 + \mathrm{erf}\left(\left(G_d^{occup} - G_{d0}\right) / \sqrt{2} \cdot \bar{\sigma}\right)}{2} = \frac{n_r + n_t}{n_{\max}} \tag{4}$$

where G_{d0} and $\bar{\sigma}$ – the mean defect energy and the standard deviation (parameters of the normal distribution), n_r and n_t –concentrations of radial and tangential hydrides (independent

variables of the model), n_{max} – the concentration of all nucleation cites (parameter of the model).

The nucleation kinetics of new hydrides can be estimated as follows:

$$\frac{\mathrm{d}n}{\mathrm{d}t} = \int_0^{G_d^{occup}} R\left(G_d\right) \cdot \mathrm{d}G_d \tag{5}$$

The fraction of radially-oriented hydrides at each time step is given as [26]:

$$F_r = \frac{1 - f_{tex}}{1 + f_0 \exp\left(-\dfrac{\sigma \cdot \Delta\Omega}{kT}\right)} + f_{tex} \tag{6}$$

where f_0 and $\Delta\Omega$ in Eq. (6) are model parameters, f_{tex} is the textural factor.

The whole equation system for precipitation and growth or dissolution of hydrides are:

Precipitation and growth, $C_s\left(T\right) > \mathrm{TSSP}\left(T\right)$: Dissolution, $C_s\left(T\right) < \mathrm{TSSD}\left(T\right)$:

$$\begin{cases} \dfrac{\mathrm{d}C_s}{\mathrm{d}t} - \dfrac{1}{\tau_0}\left(C_s - C_e\right) = 0 \\ \dfrac{\mathrm{d}\theta}{\mathrm{d}t} = -\dfrac{F_r - \theta}{C_{tot} - C_s} \cdot \dfrac{\mathrm{d}C_s}{\mathrm{d}t} \\ \dfrac{\mathrm{d}n_r}{\mathrm{d}t} = F_r \int_0^{G_d^{occup}} R\left(G_d\right) \cdot \mathrm{d}G_d \\ \dfrac{\mathrm{d}n_t}{\mathrm{d}t} = \left(1 - F\right)_r \int_0^{G_d^{occup}} R\left(G_d\right) \cdot \mathrm{d}G_d \end{cases} \qquad \begin{cases} \dfrac{\mathrm{d}C_s}{\mathrm{d}t} - \dfrac{1}{\tau_0}\left(C_s - C_e\right) = 0 \\ \dfrac{\mathrm{d}\theta}{\mathrm{d}t} = 0 \\ \dfrac{\mathrm{d}n_r}{\mathrm{d}t} = 0 \\ \dfrac{\mathrm{d}n_t}{\mathrm{d}t} = 0 \end{cases} \tag{7}$$

Furthermore, the concentration of radial and tangential hydrides n_r and n_t is reduced to zero with a characteristic diffusional time if the temperature exceeds the temperature of the total dissolution of all hydrides.

It is assumed that neither dissolution nor precipitation occurs for hydrides if $\mathrm{TSSD}(T) < C_s(T) < \mathrm{TSSP}(T)$ (solubility hysteresis). In this condition, all independent variables are assumed to be constants.

2.2 The MORPHYD simulation tool

The second model used for the simulation of hydride morphology is a MORPHYD (an acronym of MORPHology of HYDrides), which is available online for free and described in publications [27] and [28]. The fundamental concept of this approach is to simulate a random nucleation and growth of hydrides in a three-dimensional domain in order to predict the connectivity metrics of hydrides. The cross-section of the virtual domain is assumed to be analogous to the metallographic section employed in experimental studies of hydrides. Consequently, this simulation approach is capable of estimating any morphology metric that could be determined from micrographs. Furthermore, the mass simulations of small volumes permit the estimation of the statistical distribution of these morphology metrics based on the Monte Carlo method.

The physical model of the second simulation approach is identical to that of the first, assuming heterogeneous nucleation and diffusion growth of disc-shaped hydrides, which can have one of two possible orientations. However, the general mathematical description and numerical implementation are distinct. The MORPHYD model considers a three-dimensional domain with pre-defined hydride nucleation sites. The spatial distribution of the nucleation sites and their distribution by defect energies can be determined by the user. The default parameters are a uniform spatial distribution in a cubic lattice and a normal distribution by energy. The probability of nucleation at each time step for each defect is estimated as $r \cdot \tau$, where τ is the time step, $r = R/N$ with R – the nucleation rate as defined by Eq (2). The orientation of the new hydride is a stochastic value. The probability of the hydride to have radial orientation is F_r and $(1 - F_r)$ represents the probability of tangential orientation. F_r is determined by Eq. (6).

The growth of nucleated hydrides is supported by the diffusion sink from the solid solution. Once nucleated hydrides "compete" for the hydrogen in solid solution needed for their

growth with their neighbors, this "competition" causes hydrides randomly nucleated as a cluster to be shorter than isolated hydrides randomly nucleated far from neighbors. The "clustering effect" exerts a significant influence on the morphology of hydrides, and is therefore taken into account in simplified approaches that avoid the solution of 3D diffusional tasks.

The simplified approach accounting for the "clustering effect" is based on the Voronoi tessellation [42]. The Voronoi cell for each hydride is defined as the ensemble of points for which the center of the hydride is closer to the center of any other hydride. The example of a three-dimensional Voronoi tessellation for nine hydrides in a domain is shown in Fig. 1. For further diffusional growth of hydrides, it is assumed that each hydride can absorb only hydrogen from its Voronoi cell, which limits its growth. However, as the sink for solute hydrogen atoms is the edge of the hydride (or its surface), but not its center, as is assumed, the approach based on Voronoi tessellation is only valid for small hydrides, which are much smaller than the size of their Voronoi cell.

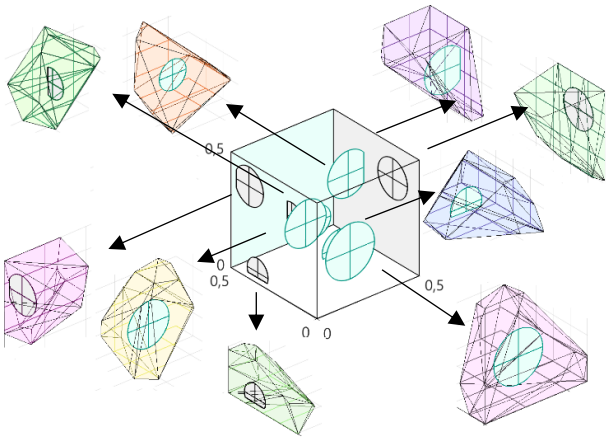

Fig. 1. Hydrides as discs in 3D domain 0.5x0.5x0.5 mm and their Voronoi cells

In its current application, the MORPHYD tool is unable to simulate the dissolution of hydrides, but only nucleation and growth. Consequently, it is currently employed for modelling samples with total dissolution of hydrides and only during cooling from the solid solution.

3. Simulations of morphology in SPIZWURZ bundle tests

3.1 Experimental conditions

The thermomechanical conditions in the SPIZWURZ bundle test were designed to simulate the long-term dry storage of spent nuclear fuel. The samples were unirradiated commercial rod claddings from Zircaloy-4, opt. ZIRLO and DUPLEX DX-D4 alloy, with an approximate length of 2.5 m loaded by internal gas pressure. They were hydrogenated to achieve target values of 100 or 300 ppm, which are in the range of typical values for high-burnup fuel and allow to compare the hydride reorientation behavior in samples with total (100 ppm) and partial (300 ppm) hydride dissolution. These two different situations are of interest for modelling. Twenty-one samples were combined into a bundle and subjected to a heating and subsequent stepwise cooling process over a period of approximately 250 days. The temperature field within the bundle was monitored using thermocouples in 15 axial zones, with the temperature history in the hottest axial zone presented in Fig. 2 (left). The stepwise cooling was performed with the slowest technically possible cooling rate: ~ 0.04 ºC/h (~ 1 ºC/day) as the mean value and ~5 ºC/h as the maximum value.

In the presented simulation, the hydride morphology was only simulated in two Zircaloy-4 samples (rods 2 and 8) differed in their hydrogen concentrations and chosen from the hottest axial zone. Both rods were symmetrically placed in the bundle, ensuring that their temperature histories were identical. The internal pressure was also almost identical, with a value of approximately 146 bar and a constant level throughout the test, as illustrated in Fig. 2 (right). The hydride morphology at the end of the test is illustrated in Fig. 3. Hydrides can be seen here as dark line segments. The thermomechanical cycle resulted in partial reorientation of the hydrides compared to the initial 100% circumferential orientation. These micrographs

were employed to quantify the main morphology metrics and subsequently to compare them with the calculated values.

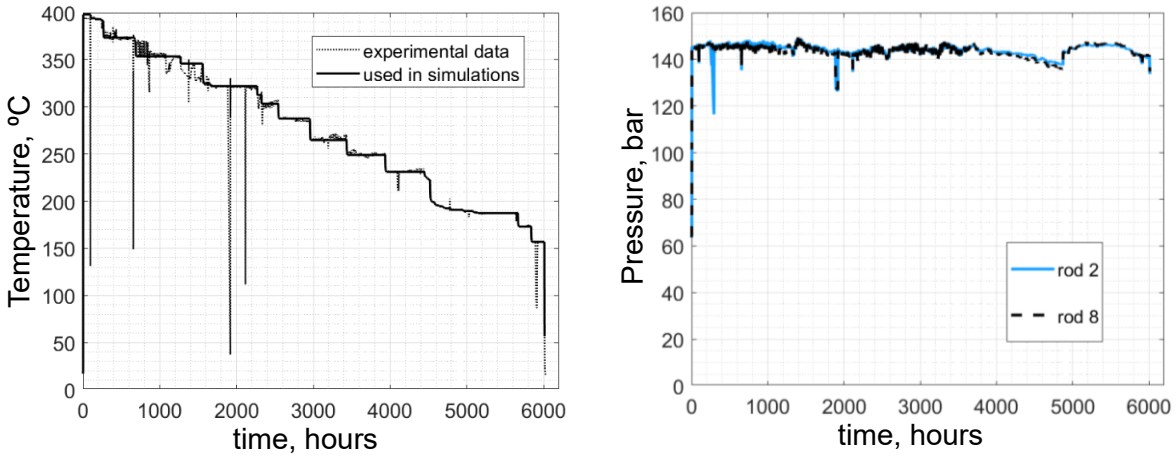

Fig. 2. History of temperature (left) in the hottest axial zone and internal pressures (right)

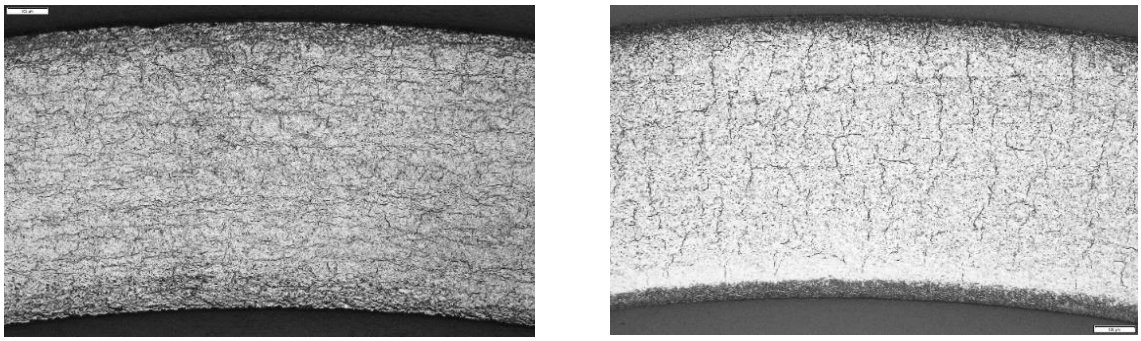

Figure 3 –Hydride morphology in rod 2 (left, 300 ppm) and rod 8 (right, 100 ppm)

3.2 Comparison of simulation and experimental results

The comparison of the main parameters calculated by the models and measured in the experiments is presented in Tables 1 and 2. The experimental RHF and RHCP was estimated by the micrograph analysis program described in [15]. The experimental mean hydride length, the hydride length distribution and density of hydrides at the micrograph was measured manually (the number of hydrides per micrograph is almost the same if measure it by the code [15]). The agreement between calculation results and experimental data is considered acceptable, especially for RHF. The coupled simulation of nucleation and diffusion growth of hydrides will be calibrated in the future as new experimental data become available (including data from the SPIZWURZ project), which are expected to allow the mean length and density of hydrides to be simulated with greater accuracy.

Rod	H ppm	RHF		mean length of hydrides, μm		density of hydrides at the micrograph, m^{-2}	
		exp.	calc.	exp.	calc.	exp.	calc.
2	300	0.21	0.26	40	33*	$4.5 \cdot 10^8$	$4.7 \cdot 10^{8*}$
8	100	0.58	0.56	31.5	41.3	$3.3 \cdot 10^8$	$1.2 \cdot 10^8$

* Results are determined by the initial state

Tab. 1: The main parameters of hydrides morphology (mean values) in the end of the test in the axial zone with the maximal temperature. Calculated by a model described in Section 2.1 and [26]

The simulation demonstrated no new hydrides nucleation during cooling in rod 2 with 300 ppm, which exhibited only partial dissolution at the maximal temperature. Consequently,

the hydride density and mean length of hydrides at the end of the test are contingent upon the initial conditions in rod 2. By contrast, rod 8 with 100 ppm experienced a total dissolution of hydrides, and the resulting hydride density and length are almost independent on the initial state and determined by the balance between nucleation frequency and the efficiency of the diffusional flow defining the nucleation time. As only rod 8 experienced the full dissolution of hydrides, it was independently simulated with the MORPHYD tool to simulate the connectivity metric RHCP and the statistical distribution of RHCP and hydride lengths.

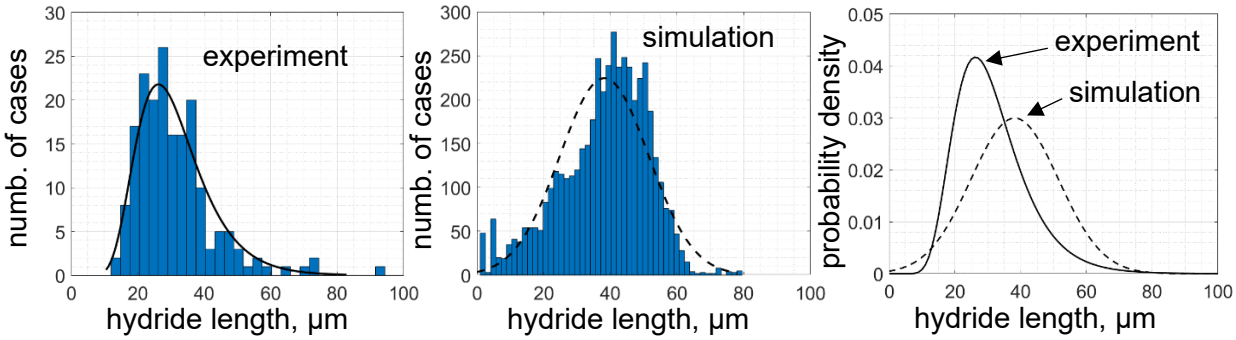

Figure 4 – Statistical distribution of hydride lengths in experiment (solid line) and as a result of simulations (dotted line) after tests in rod 8

Rod	H ppm	RHCP*			
		exp. value	mean value, calc.	Parameters of Beta-distribution (calc.)	
				A	*B*
8	100	0.32	0.32	13.43	28.7

*RHCP was determined in calculations on an area 0.5 x 0.7 mm^2

Tab. 2: Comparison of RHCP metric calculated by a model described in Section 2.2 and measured in experiment with [15]

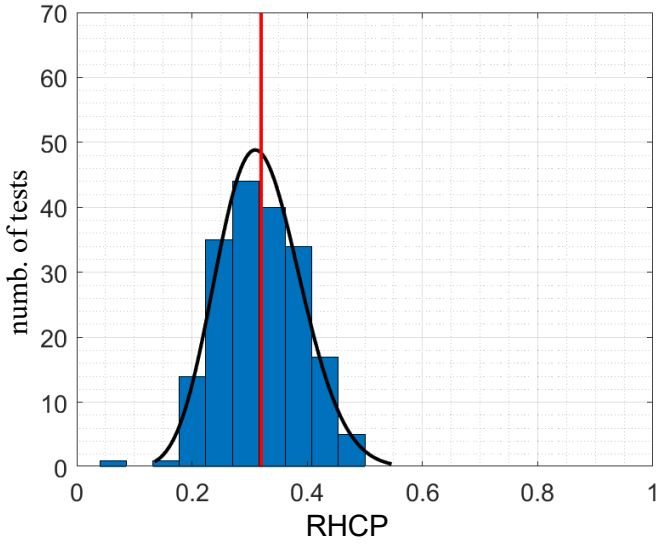

Figure 5 – Statistical distribution of RHCP metric in a random micrograph 0.5x0.7 mm^2 as a result of simulations of rod 8. The experimental value is marked as a vertical line

The hydride length distributions from the experimental micrograph and those calculated with the MORPHYD tool are compared in Fig. 4. The mean value and the distribution width are found to be similar. However, there is a notable difference between the experimental and calculated distributions. The experimental distribution fits well with a lognormal function, while the calculated distribution does not, and the universal normal distribution was used to estimate the mean and width of the calculated distribution. This discrepancy may be attributed to the numerical implementation of the model and the assumption that nucleation sites have a regular

cubic lattice. Further studies in this area are planned following the receipt of additional experimental data from the SPIZWURZ project.

Statistical distribution of RHCP metric was built up by the results of around two hundreds of independent simulations. The number of simulations is considered to be statistically representative as it gives a smooth distribution of results as seen in Fig. 5. It was compared with only one experimental value currently available in Table 2 and Fig. 5. The measured value is equal to the maximum value of the probability density function for RHCP.

4. The problem of small samples

Hydrides connectivity is a local metric, especially, at low hydrogen concentrations and cooling rates, when the hydrides are long and spaced. In fracture testing with small samples, such as the ring tensile test, where deformation is localized in a small volume, there is no guarantee that the most detrimental morphology of the hydrides will accidentally be in the fracture area. The probability p_{crit} to find the critical value of the hydride morphology metric (say, RHCP) in a small volume Ω can be estimated as:

$$p_{crit} = 1 - \left[\int_0^{RHCP_{crit}} \mathrm{PDF}\left(RHCP\right) \cdot \mathrm{d}RHCP \right]^{\Omega/V_0} \tag{8}$$

where PDF – the probability density function determined by calculations or experiments, V_0 – the volume defining the PDF (~ 0.5 mm x 0.7 mm x hydride length for data in Tab. 2 and Fig. 5 here).

5. Conclusion

The evolution of hydride morphology in conditions of the SPIZWURZ bundle test was simulated by two independent numerical tools and compared with the initial experimental results for two Zircaloy-4 samples hydrogenated up to 100 and 300 ppm. Theoretical approaches showed acceptable agreement with experiments for several hydride morphology metrics, including: radial hydride fraction, hydride density, mean hydride length and hydride length statistical distribution and connectivity of hydrides (RHCP). Further model adjustments are planned following the receipt of additional experimental data from the SPIZWURZ project. As the bundle test provided numerous and varied material on temperature history and different alloys (in particular showing different creep), the corresponding modelling will be continued with additional specimens and axial zones.

6. References

[1] B. F. Kammenzind *et al.* in *Zircon. Nucl. Ind. 11th Int. Symp., ASTM STP1295*, 1996, p. 338, DOI: 0.1520/STP16180S

[2] M.C. Billone *et al.*, *J. Nucl. Mater.*, 433 (2013) 431–448, DOI: 10.1016/j.jnucmat.2012.10.002

[3] Q. Auzoux *et al.*, *J. Nucl. Mater.*, vol. 494, p. 153893, 2022, doi: 10.1016/j.jnucmat.2022.153893

[4] M. C. Billone *et al*., SFWD-SFWST-2017-000001, 2017, DOI: 10.2172/1478471

[5] M. Kolesnik, *Eng. Fail. Anal.*, 108110, 2024, DOI: 10.1016/j.engfailanal.2024.108110

[6] Q. Fang *et al. Mater. Charact.*, 134 (2017) 362–369, DOI: 10.1016/j.matchar.2017.11.013

[7] J. Li *et al. Int. J. Fatigue*, 129 (2019) 105230, DOI: 10.1016/j.ijfatigue.2019.105230

[8] W. Xufeng *et al.*, *J. Mater. Eng. Perform.*, 10, 2023, DOI: 10.1007/s11665-023-09006-w

[9] D. Hardie and M. W. Shanahan, *J. Nucl. Mater.*, 55 (1975) 1–13, DOI: 10.1016/0022-3115(75)90132-4

[10] S.J. Min *et al. J. Nucl. Mater.*, 441 (2013) 306–314, DOI: 10.1016/j.jnucmat.2013.06.006.

[11] M. Maric *et al.*, *Zircon. Nucl. Ind. 20th Int. Symp.* 2023 639–672 DOI: 10.1520/stp164520220051

[12] R.K. Sharma *et al. J. Nucl. Mater.* 508 (2018) 546–555 DOI: 10.1016/j.jnucmat.2018.06.003

[13] A. Gopalan *et al.*, *J. Nucl. Mater.*, 544 (2021) 152681, DOI: 10.1016/j.jnucmat.2020.152681

[14] M.Nakatsuka and S Yagnik, *J. ASTM Int.*, 8 (2010) JA102954, DOI: 10.1520/JAI102954.

[15] P.C.A. Simon *et al. J. Nucl. Mater.* 547 (2021) 152817 DOI: 10.1016/j.jnucmat.2021.152817
[16] M. Maric *et al.*, *J. Nucl. Mater.*, 559 (2022) 153442 DOI: 10.1016/j.jnucmat.2021.153442
[17] D.Kim *et al. J. Nucl. Mater.* 564 (2022) 153647, DOI: 10.1016/j.jnucmat.2022.153647
[18] C. E. Ells, *J. Nucl. Mater.*, 35 (1970) 306–315, DOI: 10.1016/0022-3115(70)90214-X
[19] K. S. Chan *J. Nucl. Mater.* 227 (1996) 220–236 DOI: 10.1016/0022-3115(95)00160-3
[20] J. Y. R. Rashid and A. J. Machiels, *The 10th Int. Conf. on Environmental Remediation and Radioactive Waste Managment, ICEM05-1038*, 2005, ICEM05-1038
[21] A. R. Massih and L. O. Jernkvist, *Comput. Mater. Sci.*, 46 (2009) 1091–1097, DOI: 10.1016/j.commatsci.2009.05.025
[22] M. Kolesnik *et al*. *J. Nucl. Mater.* 508 (2018) 567–573 DOI: 10.1016/j.jnucmat.2018.06.012
[23] J. Desquines *et al.*, *J. Nucl. Mater.*, 453 (2014) 131–150, DOI: 10.1016/j.jnucmat.2014.06.049
[24] F. Feria *et al.*, *Ann. Nucl. Energy*, 145 (2020) 107559, DOI: 10.1016/j.anucene.2020.107559
[25] P.Konarski *et al. Nucl. Eng. Technol.* 56 (2024) 728–744 DOI: 10.1016/j.net.2023.11.012
[26] M. Kolesnik *et al.*, *Comput. Mater. Sci.*, 189 (2021) 110260, DOI: 10.1016/j.commatsci.2020.110260
[27] M. Kolesnik *et al. Phys. Met. Metall.*, 104 (2023), DOI: 10.1134/S0031918X22602074
[28] T. Aliev and M. Kolesnik, *Lett. Mater.*, 13 (2023) 143–148, DOI: 10.22226/2410-3535-2023-2-143-148
[29] J. Stuckert, C. Rössger, J. Moch, M. Grosse, and S. Weick, 28th Int. QUENCH Worckshop, 2023, DOI: 10.5445/IR/1000168767
[30] M.Grosse *et al. Nucl. Eng. Technol.* 56 (2024) 824–831 DOI: 10.1016/j.net.2023.09.027
[31] A. McMinn *et al.*, *Zircon. Nucl. Ind. 12th Int. Symp.*, 1354 (2000) 173–195, DOI: 10.1520/stp14300s
[32] P. Vizcaíno *et al*., *J. Nucl. Mater.*, 304 (2002) 96–106, DOI: 10.1016/S0022-3115(02)00883-8
[33] P. Vizcaíno *et al*., *J. ASTM Int.*, 8 (2011) 1–20, DOI: 10.1520/JAI102949
[34] B. F. Kammenzind and W. J. Duffin, *Zircon. Nucl. Ind. 18th Int. Symp.*, 2018, DOI: 10.1520/STP159720160060
[35] H. M. Nordin *et al.*, *J. Chem. Inf. Model.*, 53 (2017) 1689–1699, DOI: 10.1017/CBO9781107415324.004
[36] K.N. Jang and K. T. Kim, *Nucl. Eng. Technol.*, 49 (2017) 1472–1482, DOI: 10.1016/j.net.2017.05.006
[37] R. S. Daum *et al*., *J. Nucl. Sci. Technol.*, 43 (2006) 1054–1067, DOI: 10.1080/18811248.2006.9711195
[38] P. Bouffioux *et al.*, *LWR Fuel Perform. Meet. Top Fuel 2013*, 879–886
[39] J. S. Kim and Y. S. Kim, *Int. J. Hydrogen Energy*, 39 (2014) 16442–16449, DOI: 10.1016/j.ijhydene.2014.08.018
[40] J.J. Kearns *J. Nucl. Mater.* 43 (1972) 330–338, DOI: 10.1016/0022-3115(72)90065-7
[41] H. I. Aaronson, M. Enomoto, and J. K. Lee, *Mechanisms of Diffusion Phase Transformations in Metals and Alloys*. CRC Press, 2010
[42] G. Voronoi, *J. Reine Angew. Math.*, 133 (1908) 97–178